

## RESEARCH PAPER

## Synthesis and cytotoxicity analysis of fatty acid-mediated maghemite nanoparticles in cancerous and normal cells

Mina Zangouei<sup>1,2</sup>, Elham Einafshar<sup>3,4</sup>, Fatemeh Forouzanfar<sup>5,6</sup>, Tayebeh Hamzehloei<sup>1,7</sup>, Zahra Meshkat<sup>8</sup>, Aida Gholoobi<sup>7,1\*</sup>

<sup>1</sup> Medical Genetics Research Center, Mashhad University of Medical Sciences, Mashhad, Iran

<sup>2</sup> Department of Biology, Faculty of Science, Ferdowsi University of Mashhad, Iran

<sup>3</sup> Pharmacological Research Center of Medicinal Plants, Mashhad University of Medical Sciences, Mashhad, Iran

<sup>4</sup> Department of Pharmacology, Faculty of Medicine, Mashhad University of Medical Sciences, Mashhad, Iran

<sup>5</sup> Neuroscience Research Center, Mashhad University of Medical Sciences, Mashhad, Iran

<sup>6</sup> Department of Neuroscience, Faculty of Medicine, Mashhad University of Medical Sciences, Mashhad, Iran

<sup>7</sup> Metabolic Syndrome Research Center, Mashhad University of Medical Sciences, Mashhad, Iran

<sup>8</sup> Antimicrobial Resistance Research Center, Mashhad University of Medical Sciences, Mashhad, Iran

### ABSTRACT

**Objective(s):** Our goal was to synthesize and characterize fatty acid-capped maghemite nanoparticles (NPs) and evaluate their cytotoxic effect on human cancer and normal cell lines.

**Methods:** Maghemite NPs were synthesized by co-precipitating iron (II) chloride tetrahydrate and iron (III) chloride hexahydrate, followed by surface capping with monounsaturated fatty acid, named oleic acid (OA). The particles were characterized using X-ray diffraction (XRD), field-emission scanning electron microscopy (FE-SEM), transmission electron microscopy (TEM), energy-dispersive X-ray spectroscopy (EDS), vibrating-sample magnetometer (VSM), and Fourier-transform infrared spectroscopy (FTIR). The cytotoxicity of the capped NPs was assessed using an MTT assay.

**Results:** XRD analysis confirmed the formation of highly crystalline maghemite NPs with a cubic structure and an estimated crystallite size of approximately 9 nm. FE-SEM and TEM images revealed semi-spherical and cuboidal particles with an average size of 14 nm. EDS analysis confirmed the presence of iron, oxygen, carbon, and gold elements. VSM analysis demonstrated a saturation magnetization value of about 51 emu/g, while FTIR confirmed the successful capping of maghemite NPs with OA. The MTT assay showed that the NPs exhibited no cytotoxic effects on CaSki or HUVEC cells, even at the highest 50 µg/mL concentration.

**Conclusion:** The synthesized OA-capped maghemite NPs exhibited promising superparamagnetic properties with no significant cytotoxic effects on human cancer or normal cell lines, suggesting potential applications in biomedicine.

**Keywords:** Iron oxide nanoparticles; Oleic acid; Stabilizers; Cell survival; Biocompatibility

### How to cite this article

Zangouei M, Einafshar E, Forouzanfar F, Hamzehloei T, Meshkat Z, Gholoobi A. Synthesis and cytotoxicity analysis of fatty acid-mediated maghemite nanoparticles in cancerous and normal cells. *Nanomed J.* 2025; 12(3):518-528. DOI: [10.22038/nmj.2025.81397.2020](https://doi.org/10.22038/nmj.2025.81397.2020)

### INTRODUCTION

With recent developments in nanotechnology, magnetic iron oxide nanoparticles (Fe<sub>3</sub>O<sub>4</sub> and γ-Fe<sub>2</sub>O<sub>3</sub> NPs) have attracted considerable interest (1, 2). Specifically, comprehensive studies have been dedicated to the various potential applications of maghemite (γ-Fe<sub>2</sub>O<sub>3</sub>) NPs. In medical investigations, the focus has been on targeted release (3), cancer hyperthermia (4), radionuclide treatment (5), diagnostics (4), and, more recently, evaluated for

magnetic resonance imaging (MRI) contrast applications (6). In particular, the size of NPs and their low toxicity are significant characteristics in regulating materials' magnetic behavior under *in vivo* settings, which can profoundly affect their biomedical applications (7, 8). Chemical co-precipitation is the prevailing method for preparing magnetic iron oxide NPs with meticulous control over the size, size distribution, and shape of the particles, using moderate temperature conditions (9). In addition, the potential long-term toxicity of NPs in biological systems is an important issue that needs to be investigated (10). Selecting a proper capping agent is one of the practical ways to

\*Corresponding author(s) Email: [gholoubiad@mums.ac.ir](mailto:gholoubiad@mums.ac.ir).

Note. This manuscript was submitted on July 07, 2024; approved on September 28, 2024

overcome the cytotoxicity of NPs. It can act as a suitable stabilizer and increase absorption by living cells. In order to be efficiently utilized by the biological system, capping agents should be biodegradable, readily dispersed, biocompatible, and non-toxic. They reduce adventitious adhesion to biological components, lowering cellular toxicity (10). Oleic acid (OA) belongs to the omega-9 fatty acid monounsaturated and is present in various animal and plant sources, particularly abundant in olive oil, and can be pinpointed as a capping agent (11). Besides, OA is regarded to be highly oxidation-resistant and can enhance the antioxidant effect of tocopherols. It can have an immunomodulatory effect and prevent various diseases, including cardiovascular or autoimmune diseases, metabolic abnormalities, skin damage, and cancer. It also has a remarkable impact on the absorption of medications (11, 12).

The capping method plays a crucial role in enhancing the stability and functionality of NPs. By forming a protective layer around the NPs, capping prevents oxidation and degradation, thereby preserving their magnetic properties and overall stability. This method also ensures consistent dispersion of the NPs, improving their solubility in various solvents and facilitating their incorporation into different formulations. Moreover, capping prepares NPs for potential further functionalization, enabling them to retain their core properties while being adaptable to specific biomedical applications (13-15). In our research, maghemite NPs were synthesized using co-precipitation and then capped with OA to mitigate the potential adverse effects of using these particles. The produced capped-maghemite NPs with OA are proven superparamagnetic iron oxide NPs (SPIONs) via vibrating sample magnetometer (VSM) analysis. We also characterized the crystal structure, morphology, functional groups, and cytotoxicity. For this purpose, we used X-ray diffraction (XRD), field-emission scanning electron microscopy (FE-SEM), energy dispersive X-ray spectroscopy (EDS), transmission electron microscopy (TEM), Fourier transform infrared spectroscopy (FTIR), and toxicity assessment throughout our experiments.

## MATERIALS AND METHODS

### Materials

Iron (III) chloride hexahydrate (98%) and iron (II) chloride tetrahydrate (99%) (Sigma-Aldrich, Germany) were purchased as iron sources.  $\text{NH}_4\text{OH}$  solution (25 Vol%, Merck) and OA (90%) (Sigma St. Louis, MO), functioned as a pH modifier and surface

stabilizer, respectively. Furthermore, the cancer human papillomavirus type 16 positive epithelial (CaSki) cell line and normal human umbilical vein endothelial (HUVEC) cell line were bought from the CLS and Pasteur Institute. Tetrazolium salt was purchased from Sigma-Aldrich (Saint Louis, MO, USA). Cultured cells were grown in RPMI 1640 culture medium supplemented with 10% heat-inactivated fetal bovine serum (Gibco), penicillin (100 IU/mL), and streptomycin (100 mg/mL) (Invitrogen). Each material and reagent was used without further purification.

### Preparing the maghemite nanoparticles

We synthesized capped-maghemite NPs based on our previous study (16). Briefly, maghemite NPs were made by co-precipitating iron (II) chloride tetrahydrate (12 g) and iron (III) chloride hexahydrate (24.3 g). They were mixed in 50 mL of water (deionized) in a 3-mouth flask under argon gas for 30 minutes at ambient temperature. Afterward, the flask was put in an 80°C water bath, and 35 mL of 28% ammonium hydroxide was added dropwise under a magnetic stirrer. Fifteen mL of OA was then added drop-by-drop for 10 minutes, followed by 30 minutes of continuous stirring at 80°C. The mixture was stirred until all the ammonium evaporated. Finally, a magnet separated the black sediment, which was centrifuged at a relative centrifugal force of approximately  $15,652 \times g$  with a rotor radius of 14 cm for 15 minutes and triple-washed with water and acetone. The last wash with 50°C water removed the excess OA. The NPs were lyophilized at -60°C for two days under seven mm Hg pressure.

### Characterization of prepared nanoparticles

The prepared capped-maghemite NPs with OA were characterized using XRD (PW 3040/60, X Pert PRO; Netherland), FE-SEM (Mira 3-XMU), TEM (FEI Tecnai F20, Philips Electron Optics, Holland), and FTIR ((Shimadzu 8400, Japan). A vibrating sample magnetometer was employed to measure the magnetic behavior (VSM, AGFM/VSM 3886 Kashan, Iran) under ambient conditions with a 1.0 T magnetic field applied

### Cytotoxicity assessment

A tetrazolium salt reduction test was used to measure the toxicity of capped-maghemite NPs on the CaSki and HUVEC cell lines. At the bottom of two 96-well plates,  $5 \times 10^3$  cells were seeded in a 200  $\mu\text{L}$  volume of cell culture, respectively, and incubated at 37 °C, 5%  $\text{CO}_2$ , and 90% humidity for 24 h.



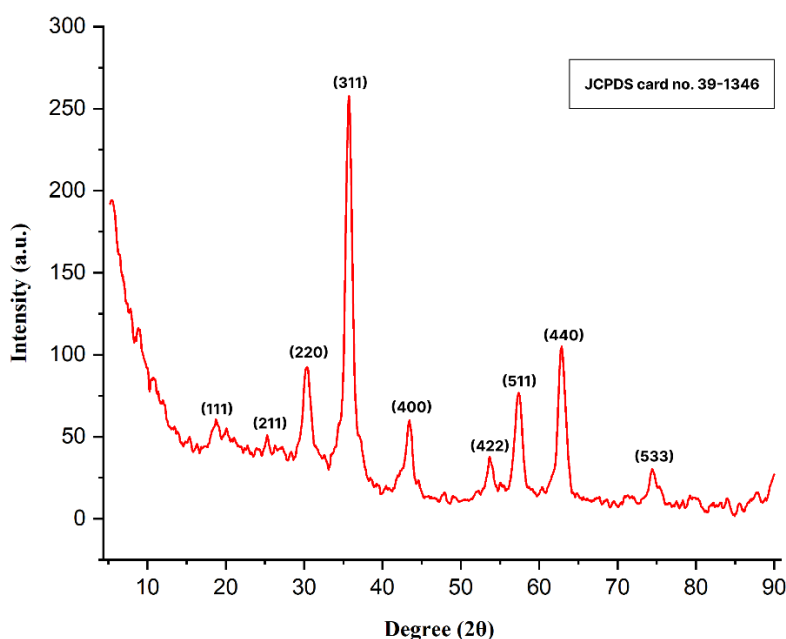


Fig. 1. XRD pattern of synthesized maghemite NPs capped with OA.

The cell culture media was withdrawn the following day, and different concentrations of capped-NPs were prepared and treated in a 200  $\mu$ L volume with cells in triplicate as follows. First, 1 mg of the NPs was dissolved in 20  $\mu$ L of DMSO through 30 minutes of sonication, and then 980  $\mu$ L of culture medium was added (1 mg/mL) and dissolved appropriately. Concentrations of 50, 25, 12.5, 6.25, 3.125, 1.56, and 0.78  $\mu$ g/mL were prepared from the stock. Besides, 200  $\mu$ L of cell culture medium was added to three wells as negative controls. They were then incubated for 24 h at 37  $^{\circ}$ C, 5% CO<sub>2</sub>, and 90% humidity. After this, the cell culture media were drained, and 20  $\mu$ L of MTT solution was added per well along with 200  $\mu$ L of the prepared culture medium. This was incubated for 3 hours at 37  $^{\circ}$ C. The formation of purple formazan crystals was investigated with a microscope. Then, the cell supernatant was slowly collected, 200  $\mu$ L of DMSO was added, and the crystals were dissolved. The optical absorbance of the plates was read at a wavelength of 540 nm with an ELISA reader.

## RESULTS AND DISCUSSION

### X-ray Diffraction analysis

The XRD pattern of maghemite NPs capped with OA is shown in Figure 1. As illustrated in the following figure, the XRD of synthesized capped-maghemite NPs with OA in total involves six distinct peaks (220, 311, 400, 422, 511, and 440). The NPs exhibit a high level of crystallinity, as indicated by the sharp peaks. Compared to JCPDS card No. 39-1346, the cubic structure of maghemite NPs was verified by

detecting peaks at various values. The existence of characteristic peaks of  $\gamma$ -Fe<sub>2</sub>O<sub>3</sub> at 35.46 $^{\circ}$  and 43.12 $^{\circ}$  ensures the presence of maghemite NPs (17). Moreover, bioorganic molecules on the surface of maghemite NPs may account for several unidentified extra peaks detected by XRD. They operate as reducing capping agents on the surface of  $\gamma$ -Fe<sub>2</sub>O<sub>3</sub> and give stability to maghemite NPs (18, 19). A broad peak is observable at  $2\theta = 19.7$ , which could potentially arise from the crystalline structure of the OA monolayer capped the NP's surface. An XRD pattern of pure OA displays a peak near  $2\theta = 19$ , similar to the band location detected for the capped NPs (20).

According to the Debye-Scherrer formula (21), the crystallite size (D) was approximately 9 nm.

$$D = \frac{K\lambda}{\beta \cos\theta}$$

This mathematical relationship connects D to the X-ray wavelength ( $\lambda = 0.15406$  nm), the width of the diffraction peak ( $\beta$ ), a constant ( $K = 0.94$ ) related to particle morphology and crystal orientation, and the measured diffraction angle ( $\theta$ ).

### Electron microscopic properties

Figure 2 presents FE-SEM images of maghemite NPs capped with OA, captured at various magnifications. These images reveal that the NPs exhibit a semi-spherical shape with rough surfaces and are uniformly dispersed. Analysis of the images indicates that the NPs have an average diameter of approximately 14 nm.

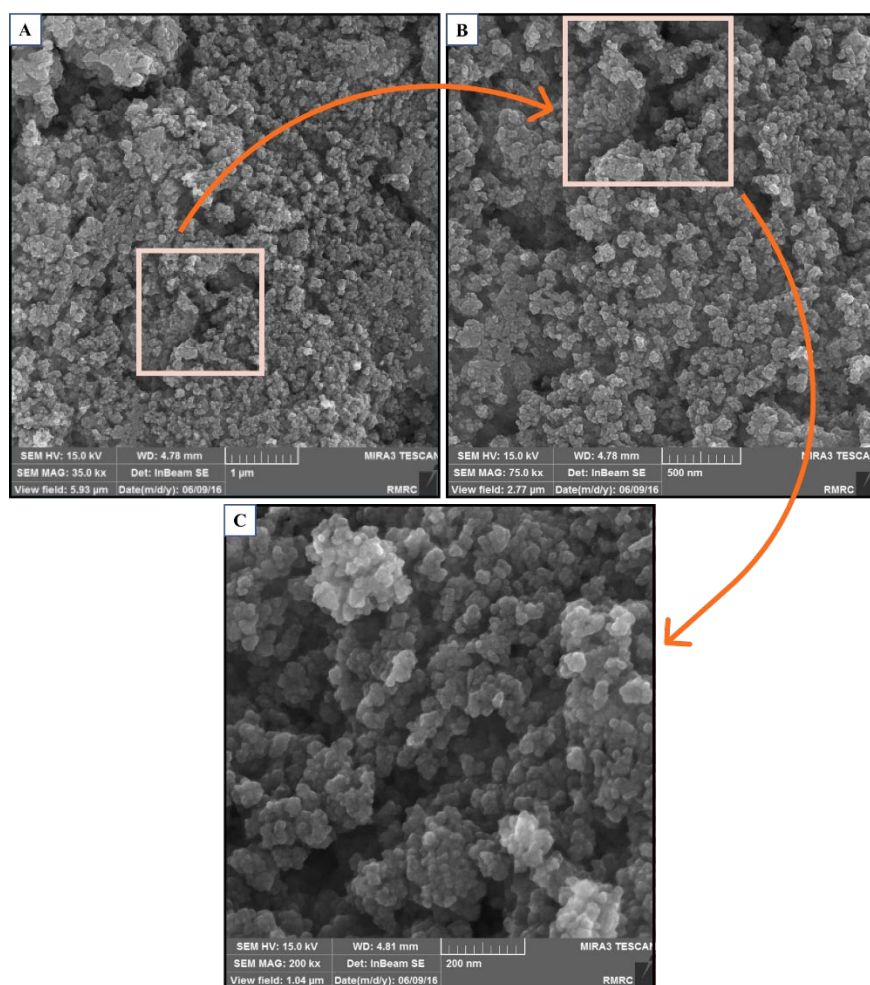


Fig. 2. FE-SEM micrographs of prepared capped-maghemite NPs with OA at various magnifications (A: 35,000, B: 75,000 and C: 200,000).

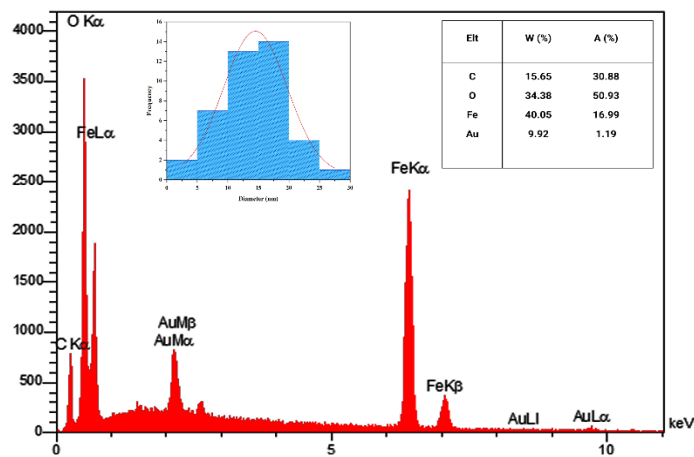


Fig. 3. EDS spectrum and average diameter of maghemite NPs capped with OA.

Table 1. Quantitative results by EDX analysis of the maghemite NPs with OA.

Elt	Line	Int	Error	K	Kr	W%	A%	ZAF
C	Ka	81.3	19.9607	0.0886	0.0559	15.65	30.88	0.3573
O	Ka	473.3	8.4349	0.2569	0.1621	34.38	50.93	0.4716
Fe	Ka	594.9	0.6407	0.5612	0.3542	40.05	16.99	0.8846
Au	La	4.4	0.3731	0.0932	0.0589	9.92	1.19	0.5933

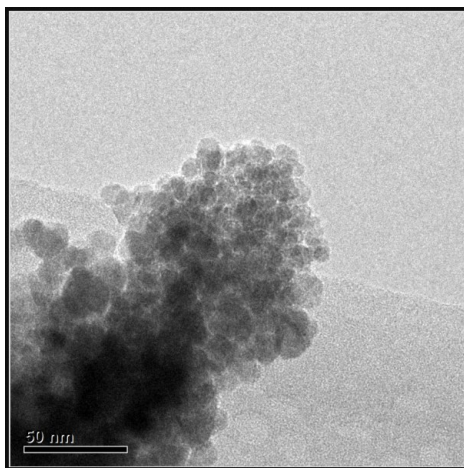


Fig. 4: TEM image of maghemite NPs stabilized with OA.

Furthermore, EDS spectroscopy was employed to identify the elemental constituents of the synthesized maghemite NPs (Figure 3, Table 1). The analysis revealed peaks for O (50.93%), C (30.88%), Fe (16.99), and Au (1.19%). Three distinctive peaks of Fe at approximately 0.5, 6.2, and 7.0 keV were observed, verifying the existence of iron in the NPs (22). Fe and O peaks were prominent in the EDS spectrum, as shown in Figure 4, further supporting the formation of maghemite NPs. Additionally, peaks for Au and C were detected, with Au resulting from the NPs' preparation for EDS analysis and C indicating the presence of OA, as indicated by FTIR. These C molecules cap NPs of maghemite.

Additionally, TEM analysis was conducted to validate the shape, size, and structure of the synthesized NPs (Figure 4). TEM images showed aggregation of 50 nm spherical particles and NPs ranging between 8 nm and 17 nm. The presence of

cuboidal-shaped particles was also observed in Figure 4.

#### **Vibrating-sample magnetometer**

Figure 5 displays the capped maghemite NPs' magnetization curve with OA, demonstrating superparamagnetic behavior with no hysteresis. The magnetization curve proves the produced NPs are SPIONs since they have exhibited superparamagnetic properties, with a magnetic saturation value of approximately 51 emu/g, according to the VSM result given in Figure 5.

#### **FTIR**

An FTIR spectrum of maghemite NPs stabilized with OA is shown in Figure 6. Based on the FTIR spectrum, it is confirmed that OA is absorbed onto the surface of the maghemite NPs. The bands at approximately 1420, 1520, and 1620  $\text{cm}^{-1}$  are

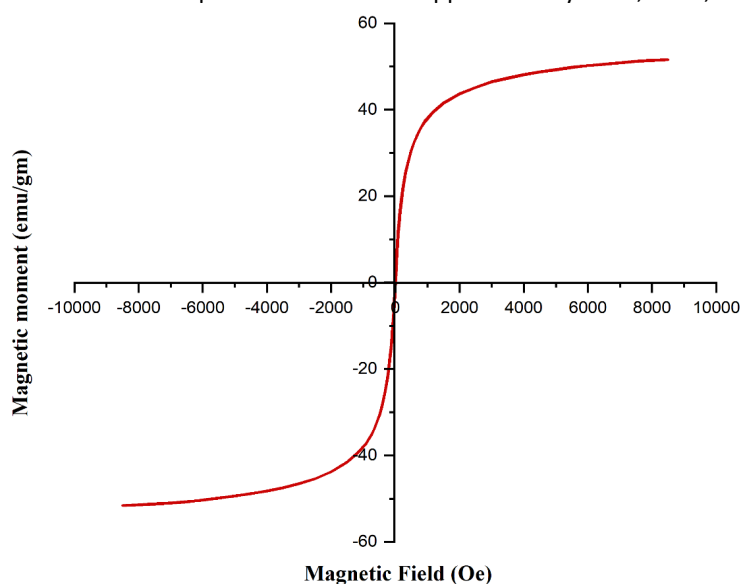


Fig. 5. Magnetization plot of synthesized capped maghemite NPs with OA at 300 K

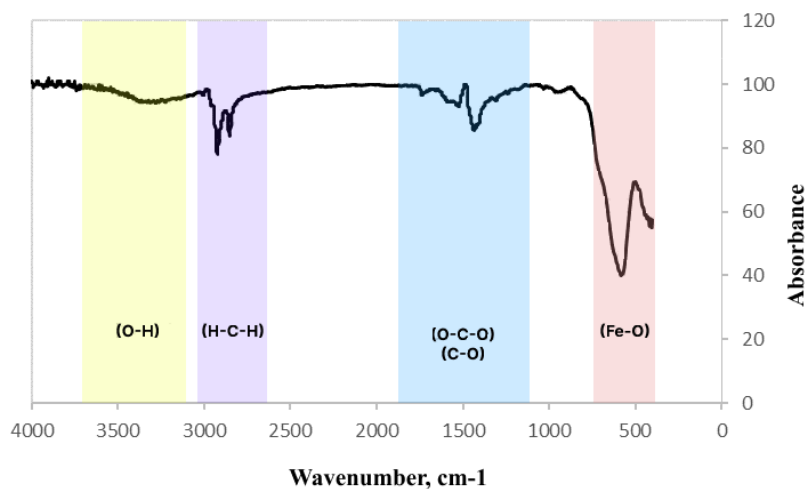


Fig. 6. The FTIR spectrum of maghemite NPs capped with OA

attributed to metal oleate. OA contains aliphatic alkyl groups. The band can be seen in the spectra below  $3000\text{ cm}^{-1}$ . There is also broadband centered at  $3350\text{ cm}^{-1}$ , which is attributed to the stretching vibration of the hydroxyl (OH) group. At approximately  $2922$  and  $3350\text{ cm}^{-1}$ , absorption bands were related to C-H and O-H (vibration mode) groups, respectively (23). A symmetric  $\text{CH}_2$  stretch and an asymmetric  $\text{CH}_2$  stretch can also be distinguished from two bands at  $2922.07$  and  $2851.23\text{ cm}^{-1}$ , respectively (24). It is evident from the analysis that a strong peak dominates the iron oxide phase at  $580\text{ cm}^{-1}$ . Moreover, the characteristic absorption bands of SPIONs at  $432$  and  $580$  can be related to the presence of the Fe-O bond.

**Prepared superparamagnetic nanoparticles cytotoxicity**

Figures 7 & 8 illustrate the toxicity of capped maghemite NPs with OA on CaSki and HUVEC cell lines. Cells were treated with different concentrations of the NPs for 24 hours, ranging from  $0$  to  $50\text{ }\mu\text{g/mL}$ . The MTT results showed no cytotoxic effects on either human cancer cells or normal cells, even at the highest dosage of  $50\text{ }\mu\text{g/mL}$ . Statistical analysis did not demonstrate significant differences between the averages at each concentration for both cell lines.

Nanomaterials such as iron oxide nanoparticles (IONs) have shown great potential in various medical and healthcare functions, including cellular staining, targeted drug delivery, gene therapy,

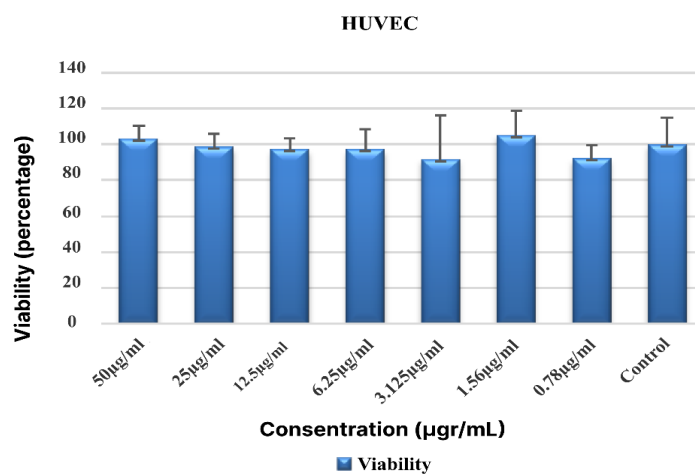


Fig. 7. Viability of HUVEC cells

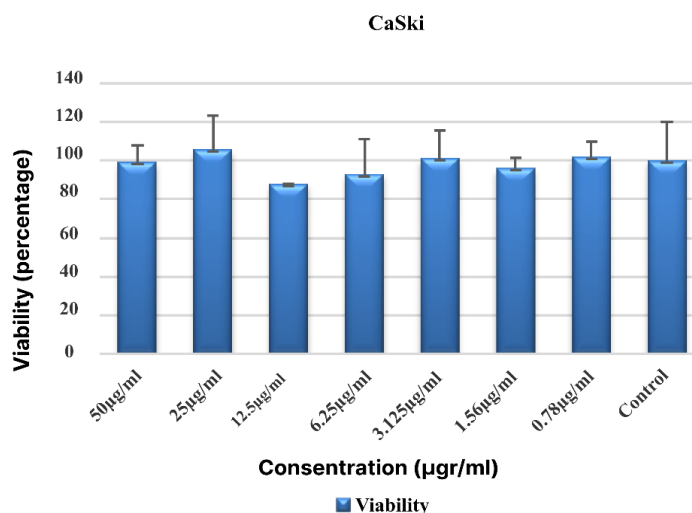


Fig. 8. Viability of CaSki cells

biosensors, hyperthermia treatment, and MRI diagnostics. These materials hold promise for treating malignant diseases and other illnesses. Nevertheless, despite the extensive exploration of IONs applications, their potential toxicity remains a subject that requires further investigation. Surface coatings and particle sizes are critical in defining cellular responses, the strength of effects induced by IONs, as well as potential toxicity pathways (25, 26).

Studies have shown that silica-coated SPIONs can induce cellular death through oxidative stress, but the addition of OA has been found to mitigate these adverse effects. OA has been shown to safeguard endothelial cells against oxidative damage and apoptosis caused by SPIONs (27), as well as changing the surface properties of IONs from hydrophilic to hydrophobic (28, 29).

In research by L. Arias and colleagues, when manufacturing (maghemite/PLGA) /chitosan (core/shell) /shell nanocomposites, this surface modification of the maghemite particles with OA facilitated their integration into the PLGA matrix. For this purpose, an ethanolic OA solution was added under sonication (30). Based on these studies, incorporating OA into the NPs synthesis introduces a distinctive element to our approach. OA, known for its environmentally friendly properties, enhances the sustainability of the NPs fabrication process. Although OA alone does not constitute a complete green synthesis method, its integration helps mitigate environmental impact while preserving the effectiveness. The use of OA not only improved the properties of the NPs but also reduced their toxicity, thereby enhancing their suitability for theranostic applications.

Saranya et al. reported a relationship between exposure time, type of cell, and the concentration of IONs in their *in vitro* studies on cytotoxicity. In this study, green IONs were also non-toxic (31). To be used in biomedical applications, magnetic NPs are preferred to exhibit superparamagnetic behavior at room temperature, have a small size of about 20 nanometers, and be biocompatible with biological coatings (32). The synthesized capped-maghemite with OA showed an efficient superparamagnetic as proved by VSM characterization. Moreover, the MTT cell viability results indicate the biocompatibility of the maghemite NPs capped with OA. These findings are consistent with prior research; for instance, Dehelean et al. obtained biocompatible colloidal suspensions from IONs synthesized by combustion of the solution and covered with an OA arrangement consisting of two layers. They confirmed that NPs had an average particle diameter between 7 and 22 nm, making them appropriate for biological purposes. *In vitro* analyses of the studied colloidal suspensions revealed no harmful effects on human keratinocyte cells' viability, proliferation, and migration (33).

Furthermore, Rahmani et al. investigated a green synthesis method for creating small-sized SPIONs and evaluated their cytotoxicity on breast cancer cells (MCF-7). They observed dose-related toxicity with mild effects at concentrations below 4.7 µg/mL (34). Similarly, Bali Ogholbeyg et al. synthesized superparamagnetic maghemite NPs using mango leaf extract and found low toxicity up to 200 µg/mL in cytotoxicity tests on MCF-7 breast cancer cells (35).

Notably, while these studies focused on cancer cells, our research included both cancer (CaSki) and normal (HUVEC) cell lines. The consistently low

toxicity observed across these different cell types reinforces the biocompatibility of the synthesized NPs (Table 2.).

Table 2. Investigation of Maghemite Nanomaterials' cytotoxicity on various cell lines

Study	Nanomaterial	Exposure Time	Cell Type	Results	Reference
Dehelean et al.	IONS NPs (maghemite & magnetite NPs coated with OA)	24 h	HaCat Cell Line	No harmful effects on the viability, proliferation, or migration of Human keratinocyte cells	(33)
Balas et al.	Dextran-coated maghemite NPs	24 h 48 h 72 h	PANC-1 Cell Line	Inhibition of PANC-1 Cell Viability in a Concentration- and Time-Dependent Manner: biocompatibility at low doses and 50% Cytotoxicity at 56 µg/mL after 72 h	(36)
Silva et al.	Methylene blue binding to citrate-coated maghemite NPs	24 h 48 h 72 h	T-47D & A2780 Cell Lines	Killing cancer cells without affecting normal cells and increasing methylene blue activity, aiming at the treatment of breast and ovarian cancer	(37)
Fernández-Álvarez et al.	(Maghemite/ PLGA)/ Chitosan Nanostructure	48 h 72 h	CCD-18 & T-84 Cell Lines	No change in the viability of both cell lines, even in the 0.05 to 100 µg/mL NP concentrations, which could be considered non-toxic	(38)
Sharifi et al.	Maghemite Nps	24 h	4T1 Cell Line	Effectiveness of NPs against cancerous cell line	(39)
Ramos-Guivar et al.	Maghemite NPs	6 h 24 h	SAOS-2 Cell Line	not reducing the cell viability even at high concentrations, enhancing the proliferation of osteoblast SAOS-2 cells compared with the untreated cells	(40)
Predoi et al.	Maghemite NPs	24 h	HepG2 Cell Line	Maintaining cell viability for up to 60 µg/ml NPs concentrations	(41)
Khodabakhshi et al.	Maghemite NPs	48 h	Hela Cell Line	Low toxicity even at high doses of NPs	(42)
Rahmani et al.	SPIONs	24 h	MCF-7 Cell Line	Low-level toxicity at concentrations under 4.7 µg/mL	(34)
Bali Ogholbeyg et al.	Maghemite NPs	24 h 48 h	MCF-7 Cell Line	Minimal toxicity on the MCF-7 breast cancer cell line (up to 200 µg/mL)	(35)
Current Study	Maghemite NPs	24 h	HUVEC & CasKi Cell Lines	Compatibility of NPs on living cell lines with no toxicity	

## CONCLUSION

In this study, maghemite NPs capped with OA were successfully synthesized using a co-precipitation method, and their properties were

comprehensively characterized. The NPs demonstrated high crystallinity and a cubic structure, with a crystallite size of approximately 9 nm. The effective capping with OA was confirmed,

resulting in semi-spherical NPs with an average size of 14 nm. Elemental analysis indicated the presence of iron, oxygen, and carbon, affirming the successful OA capping. Furthermore, the NPs exhibited superparamagnetic behavior with a saturation magnetization of approximately 51 emu/g, making them suitable for magnetic applications. Cytotoxicity assessments on CaSki and HUVEC cell lines showed no significant toxicity at concentrations up to 50 µg/mL, highlighting their biocompatibility.

Overall, the OA-capped maghemite NPs exhibit desirable properties for biomedical applications, including targeted drug delivery and imaging. Future research should focus on *in vivo* studies to comprehensively evaluate their pharmacokinetics, biodistribution, and long-term safety to realize their full potential. Additionally, exploring their efficacy in specific therapeutic areas such as targeted cancer therapy, real-time imaging, and theranostics will further validate their utility as multifunctional NPs systems in biomedicine.

#### FUNDING

This work was funded by the Mashhad University of Medical Sciences [Grant Numbers 910808, 921118].

#### CONFLICTS OF INTEREST

The authors report no relevant conflicts of interest, financial or otherwise, related to this research.

#### ETHICAL CONSIDERATIONS

The authors declare that this article does not report on any research involving human subjects or animal experiment.

#### RESEARCH DATA POLICY AND DATA AVAILABILITY STATEMENTS

The data underlying the study's results are fully available within the article and its supplementary materials, as confirmed by the authors.

#### ACKNOWLEDGMENT

We acknowledge the invaluable financial support graciously granted by the Mashhad University of Medical Sciences (Grant Numbers # 910808 and 921118).

#### AUTHORS' CONTRIBUTIONS

Mina Zangouei participated in the investigation, data curation, writing, and reviewing of the original draft. Elham Einafshar made significant contributions to the writing, editing, and reviewing of the original draft. Fatemeh Forouzanfar provided feedback and editing to refine the manuscript.

Tayebeh Hamzehloei conceptualized the research and contributed to the review writing. Zahra Meshkat was instrumental in securing funding and developing the research concept and also contributed to the review writing. Aida Gholoobi oversaw the project, developed the methodology, and contributed to the writing and reviewing of the manuscript.

#### REFERENCES

1. Ali A, Zafar H, Zia M, Haq I, Phull A, Ali J, et al. Synthesis, characterization, applications, and challenges of iron oxide nanoparticles. *Nanotechnol Sci Appl*. 2016;9:49-67.
2. Ghamari Kargar P, Maleki B, Ghani M. Ag/GO/Fe<sub>3</sub>O<sub>4</sub>/γ-Fe<sub>2</sub>O<sub>3</sub> Nanocomposite for Green-Light-Driven Photocatalytic Oxidation of 5-Hydroxymethylfurfural to 5-Hydroxymethyl-2-furancarboxylic Acid. *ACS Appl Nano Mat*. 2024;7(8):8765-8782.
3. Tietze R, Zaloga J, Unterweger H, Lyer S, Friedrich RP, Janko C, et al. Magnetic nanoparticle-based drug delivery for cancer therapy. *Biochem Biophys Res Commun*. 2015;468(3):463-470.
4. Chouhan R, Horvat M, Ahmed J, Alhokbany N, Alshehri S, Gandhi S. Magnetic Nanoparticles-A Multifunctional Potential Agent for Diagnosis and Therapy. *Cancers (Basel)*. 2021;13(9).
5. Bakht M, Sadeghi M, Pourbaghi-Masouleh M, Tenreiro C. Scope of Nanotechnology-based Radiation Therapy and Thermo-therapy. *Current Cancer Drug Targets*. 2012;12(8):998-1015.
6. Sun C, Lee JSH, Zhang M. Magnetic nanoparticles in MR imaging and drug delivery. *Adv Drug Deliv Rev*. 2008;60(11):1252-1265.
7. Bae D, Han K, Cho S, Choi S. Synthesis of ultrafine Fe<sub>3</sub>O<sub>4</sub> powder by glycothermal process. *Mater Lett*. 1998;37(4-5):255-258.
8. Chen S, Feng J, Guo X, Hong J, Ding W. One-step wet chemistry for preparation of magnetite nanorods. *Mater Lett*. 2005;59(8-9):985-988.
9. Yusefi M, Shameli K, Jumaat AF. Preparation and Properties of Magnetic Iron Oxide Nanoparticles for Biomedical Applications: A Brief Review. *J Adv Res Mater Sci*. 2020;75(1):10-18.
10. Javed R, Zia M, Naz S, Aisida SO, Ain NU, Ao Q. Role of capping agents in the application of nanoparticles in biomedicine and environmental remediation: recent trends and future prospects. *J Nanobiotechnology*. 2020;18(1):172.
11. Sales-Campos H, Souza PR, Peghini BC, da Silva JS, Cardoso CR. An Overview of the Modulatory Effects of Oleic Acid in Health and Disease. *Mini Rev Med Chem*. 2013;13(2):201-210.
12. Yousefpoor Y, Baharifar H, Esnaashari S, Gheybi F, Mehrabi M, Osanloo M, et al. A review of topical micro- and nanoemulsions for common skin diseases. *Nanomedicine J*. 2024;11(3):205-221.
13. Javed R, Zia M, Naz S, Aisida SO, Ain Nu, Ao Q. Role of capping agents in the application of nanoparticles in biomedicine and environmental remediation: recent

- trends and future prospects. *J Nanobiotechnology*. 2020;18(1):172.
14. Díez AG, Rincón-Iglesias M, Lanceros-Méndez S, Reguera J, Lizundia E. Multicomponent magnetic nanoparticle engineering: the role of structure-property relationship in advanced applications. *Mater Today Chem*. 2022;26:101220.
  15. Szczyglewska P, Feliczak-Guzik A, Nowak I. Nanotechnology-General Aspects: A Chemical Reduction Approach to the Synthesis of Nanoparticles. *Molecules*. 2023;28(13):4932.
  16. Gholoobi A, Abnous K, Ramezani M, Homaei Shandiz F, Darroudi M, Ghayour-Mobarhan M, et al. Synthesis of  $\gamma$ -Fe<sub>2</sub>O<sub>3</sub> Nanoparticles Capped with Oleic Acid and their Magnetic Characterization. *Iran J Sci Technol A*. 2017;42(4):1889-93.
  17. Rana P, Sharma S, Sharma R, Banerjee K. Apple pectin supported superparamagnetic ( $\gamma$ -Fe<sub>2</sub>O<sub>3</sub>) maghemite nanoparticles with antimicrobial potency. *Mater Sci Energy Technol*. 2019;2(1):15-21.
  18. Ansari MA, Asiri SMM. Green synthesis, antimicrobial, antibiofilm and antitumor activities of superparamagnetic gamma-Fe(2)O(3) NPs and their molecular docking study with cell wall mannoproteins and peptidoglycan. *Int J Biol Macromol*. 2021;171:44-58.
  19. Ghamari P, Maleki B, Ghani M. Fe<sub>3</sub>O<sub>4</sub>/Fe<sub>2</sub>O<sub>3</sub>/TiO<sub>2</sub>/Ag: an innovative photocatalyst under visible light irradiation in deep eutectic solvent for efficient conversion of 5-HMF to chemo-and bio-based chemicals besides their determination using HPLC. *Biomass Convers Biorefin*. 2023.
  20. Vidal-Vidal J, Rivas J, López-Quintela MA. Synthesis of monodisperse maghemite nanoparticles by the microemulsion method. *Colloids Surf A: Physicochem Eng Asp*. 2006;288(1-3):44-51.
  21. Nidhin M, Indumathy R, Sreeram K, Nair B. Synthesis of iron oxide nanoparticles of narrow size distribution on polysaccharide temolates. *Bull Mater Sci*. 2008;31:93-96
  22. Basavegowda N, Mishra K, Lee YR. Sonochemically synthesized ferromagnetic Fe<sub>3</sub>O<sub>4</sub>nanoparticles as a recyclable catalyst for the preparation of pyrrolo[3,4-c]quinoline-1,3-dione derivatives. *RSC Adv*. 2014;4(106):61660-6.
  23. Nyquist RA, Putzig CL, Kagel RO, Leugers MA. Handbook of Infrared and Raman Spectra of Inorganic Compounds and Organic Salts. *Infrared Spectra of Inorganic Compounds: Elsevier Science*; 1971.
  24. Zhang L, He R, Gu H-C. Oleic acid coating on the monodisperse magnetite nanoparticles. *Appl Surf Sci*. 2006;253(5):2611-7.
  25. Fereydouni N, Zangouei M, Darroudi M, Hosseinpour M, Gholoobi A. Antibacterial activity of chitosan-polyethylene oxide nanofibers containing silver nanoparticles against aerobic and anaerobic bacteria. *J Mol Struct*. 2023;1274:134304.
  26. Valdiglesias V, Kilic G, Costa C, Fernandez-Bertolez N, Pasaro E, Teixeira JP, et al. Effects of iron oxide nanoparticles: cytotoxicity, genotoxicity, developmental toxicity, and neurotoxicity. *Environ Mol Mutagen*. 2015;56(2):125-148.
  27. Repar N, Jovicic EJ, Kump A, Birarda G, Vaccari L, Erman A, et al. Oleic Acid Protects Endothelial Cells from Silica-Coated Superparamagnetic Iron Oxide Nanoparticles (SPIONs)-Induced Oxidative Stress and Cell Death. *Int J Mol Sci*. 2022;23(13).
  28. Matshaya TJ, Lanterna AE, Granados AM, Krause RW, Maggio B, Vico RV. Distinctive interactions of oleic acid covered magnetic nanoparticles with saturated and unsaturated phospholipids in Langmuir monolayers. *Langmuir*. 2014;30(20):5888-5896.
  29. Okassa LN, Marchais H, Douziech-Eyrolles L, Herve K, Cohen-Jonathan S, Munnier E, et al. Optimization of iron oxide nanoparticles encapsulation within poly(d,l-lactide-co-glycolide) sub-micron particles. *Eur J Pharm Biopharm*. 2007;67(1):31-38.
  30. Fernandez-Alvarez F, Caro C, Garcia-Garcia G, Garcia-Martin ML, Arias JL. Engineering of stealth (maghemite/PLGA)/chitosan (core/shell)/shell nanocomposites with potential applications for combined MRI and hyperthermia against cancer. *J Mater Chem B*. 2021;9(24):4963-4980.
  31. Saranya S, Vijayanarai K, Pavithra S, Raihana N, K. K. In vitro cytotoxicity of zinc oxide, iron oxide and copper nanopowders prepared by green synthesis. *Toxicol Rep*. 2017;4:427-430.
  32. Guardia P, Batlle-Brugal B, Roca AG, Iglesias O, Morales MP, Serna CJ, et al. Surfactant effects in magnetite nanoparticles of controlled size. *J Magn Magn Mater*. 2007;316(2):e756-e759.
  33. Coricovac DE, Moaca EA, Pinzaru I, Citu C, Soica C, Mihali CV, et al. Biocompatible Colloidal Suspensions Based on Magnetic Iron Oxide Nanoparticles: Synthesis, Characterization and Toxicological Profile. *Front Pharmacol*. 2017;8:154.
  34. Rahmani R, Gharanfoli M, Gholamin M, Darroudi M, Chamani J, Sadri K, et al. Plant-mediated synthesis of superparamagnetic iron oxide nanoparticles (SPIONs) using aloe vera and flaxseed extracts and evaluation of their cellular toxicities. *Ceram Int*. 2020;46(3):3051-8.
  35. Bali Ogholbeyg A, Kianvash, A., Hajalilou, A. et al. Cytotoxicity characteristics of green assisted-synthesized superparamagnetic maghemite ( $\gamma$ -Fe<sub>2</sub>O<sub>3</sub>) nanoparticles. *J Mater Sci Mater Electron*. 2018;29, 12135(2143).
  36. Balas M, Predoi D, Burtea C, Dinischiotu A. New Insights into the Biological Response Triggered by Dextran-Coated Maghemite Nanoparticles in Pancreatic Cancer Cells and Their Potential for Theranostic Applications. *Int J Mol Sci*. 2023;24(4).
  37. Silva A, Carvalho N, Paterno L, Moura L, Filomeno C, Paula E, et al. Methylene blue associated with maghemite nanoparticles has antitumor activity in breast and ovarian carcinoma cell lines. *Cancer Nanotechnol*. 2021;12(1).
  38. Fernandez-Alvarez F, Garcia-Garcia G, Arias JL. A Tri-Stimuli Responsive (Maghemite/PLGA)/Chitosan Nanostructure with Promising Applications in Lung Cancer. *Pharmaceutics*. 2021;13(8).

39. Sharifi M, Rezayat SM, Akhtari K, Hasan A, Falahati M. Fabrication and evaluation of anti-cancer efficacy of lactoferrin-coated maghemite and magnetite nanoparticles. *J Biomol Struct Dyn*. 2020;38(10):2945-2954.
40. Ramos-Guivar JA, Morales MA, Litterst FJ.  $\gamma$ -Fe<sub>2</sub>O<sub>3</sub> nanoparticles embedded in nanohydroxyapatite matrix for magnetic hyperthermia and in vitro osteoblast cell studies. *Ceram Int*. 2020;46(8):10658-10666.
41. Predoi D AE, Balas M, Munteanu M, Dinischiotu A. Synthesis and characterization of bio-compatible maghemite nanoparticles. *Dig J Nanomater Biostruct*. 2010; 5(3):779-786.
42. Khodabakhshi M, Bahari A. Investigation and Characterization of Maghemite ( $\gamma$ -Fe<sub>2</sub>O<sub>3</sub>) Nanoparticles and Its Cytotoxicity Studies. *Indian J Pharm Educ Res*. 2017;51(2):295-301.